Science Press

ARTICLE

Effect of Ba-Nd Composite Modification on Microstructure and Mechanical Properties of Mg-3Si-4Zn Cast Alloy

Tong Wenhui[1], Zhao Chenxi[1], Tong Fangze[3], Cai Qian[2], Huang Bonan[1], Wang Jie[1], Liu Yunyi[1]

[1] School of Materials Science and Engineering, Shenyang Aerospace University, Shenyang 110136, China; [2] Shenyang Yuchengxin Technology Service for Achievement Transformation Co., Ltd, Shenyang 110004, China; [3] Murray Edwards College, University of Cambridge, Cambridge CB3 0DF, UK

Abstract: The effects of Ba-Nd composite modification on the microstructure and mechanical properties of Mg-3Si-4Zn cast alloy were investigated. The microstructure was characterized by OM, SEM, EDS and XRD. The mechanical properties were tested by hardness test. The best modification effect was achieved when a single denaturant Ba of 1.2wt% was added to the Mg-3Si-4Zn alloy. Results show that the formed phase $BaMg_2Si_2$ can act as a heterogeneous nucleation core for the primary Mg_2Si, refining the primary Mg_2Si. Ba-Nd composite modification is achieved by adding the modifier Nd to the Mg-3Si-4Zn-1.2Ba alloy. By the calculation of the Gibbs free energy using the Miedema model and a linear fit, it is found that the growth rate of primary Mg_2Si is suppressed and the primary Mg_2Si phase in the microstructure becomes smaller because more stable compounds like $NdSi$, $NdSi_2$, Ba_2Si, and $BaSi_2$ can be formed by Nd and/or Ba atoms with Si atoms, preventing Si atoms from binding to Mg atoms at the initial stage of solidification. The best Ba-Nd composite modification effect is achieved when the Nd content is 2.0wt%, i.e. the primary Mg_2Si changes from a dendritic shape with an average area of about 600 μm^2 to a nearly square-shape with an average side length of about 5 μm and the eutectic Mg_2Si changes from complex and coarse Chinese-script shape with an average area of about 444 μm^2 to simpler shape with a mean area of about 89 μm^2. The hardness of the alloy is increased from 575.75 MPa to 612.11 MPa, increased by 6.31%.

Key words: Mg-Si-Zn alloy; Mg_2Si; Ba-Nd composite modification; microstructure; hardness; Miedema model

---

Magnesium alloy is a lightweight metallic material with excellent specific strength and stiffness, damping and shock absorption, etc. These properties give the magnesium alloy a versatile role in automotive and aerospace industries[1-3]. It can be used to manufacture products, such as vehicle seat frames, bodywork, engine block, gear shell, fairing, wingtip, owing to its lightweight[4,5]. Its application potential in these fields is of significant research value.

Magnesium has low strength and low ductility because of its hexagonal close-packed (hcp) crystal structure; therefore, it has been alloyed with other substances to produce many metallic materials with outstanding properties. However, these magnesium alloys are not perfect and their properties can be further improved by adding other substances. At first, adding Al is a strengthening method since the high solubility of Al in

magnesium can obtain the outstanding engineering properties (such as tensile strength, elongation) at room temperature in applications. Despite all these benefits, the instability of the reinforcing phase $Mg_{17}Al_{12}$ in the alloys destroys the mechanical properties (ultimate tensile strength, tensile yield strength, creep resistance, tensile and compressive creep, etc) at high temperatures, resulting in softening of the alloys beyond 125 °C[6,7]. Moreover, the increasing demands for heat resistant magnesium alloys make the poor high-temperature stability of the $Mg_{17}Al_{12}$ phase a more noticeable problem[8]. As a result, the application of the magnesium alloy strengthened with Al is restricted severely[9].

Therefore, other alloying elements that can strengthen the alloy without causing the instability of reinforcing phases are proposed, such as rare earth (RE), argentum (Ag), thorium

---

(Th) and silicon (Si) [10-13]. Many studies have shown that adding alloying elements of RE, Ag and Th to magnesium alloys can improve the high-temperature properties (high-temperature tensile strength, creep resistance) of the alloys effectively[10-12]. For example, WE 54 and WE 43 magnesium alloys strengthened with RE were developed which can work at 250~300 °C[14,15]. But these alloying elements are relatively expensive for commercial applications. In contrast, the element Si is very cheap and the intermetallic compound Mg_2Si formed in the alloys has been widely used to strengthen the aluminum alloys[16,17]. The phase of Mg_2Si obtained by adding Si elements to magnesium alloys avoids the aforementioned problems since it is a reinforcing phase with a high melting point, high hardness, low density, low expansion, and high elastic modulus[18,19]. These advantageous features make the modification effect of Mg_2Si on magnesium alloys promising in application. Although the instability of magnesium alloy at high temperatures is tackled by adding Si, the strengthening effect of Mg_2Si at room temperature is suppressed since the coarse dendritic-shaped primary Mg_2Si and the complex Chinese-script-shaped eutectic Mg_2Si can split the alloy matrix. The disturbing primary and eutectic phases of Mg_2Si are results of the facet growth of Mg_2Si and the non-equilibrium characteristics during the solidification of magnesium alloy in the standard casting process[20-22]. As a result, the room-temperature properties, especially the tensile strength and elongation, will decline significantly due to the fragmented magnesium alloy matrix by the Mg_2Si phase with angular morphologies. Refining the size and the morphologies of the primary and eutectic Mg_2Si phases becomes a critical issue.

There are many methods to refine Mg_2Si, such as heat treatment, hot extrusion and ageing, friction stirring process (FSP) and mechanical ball milling[23-26]. Studies are also conducted to assess the effects of modified melt procedures on refining Mg_2Si phases. Hot extrusion or friction stirring is limited because of the poor ductility of the magnesium alloy with high Si content. There are only minor effects of heat treatment on the eutectic Mg_2Si and scarce effects on the primary Mg_2Si[23].

Current studies on refining the structure of Mg_2Si also emphasize on modifying the alloy melt. Modification is a method of refining alloys' microstructure by adding some elements, which can be attached to the surface of the solidified crystals to prevent the growth of these crystals. Alternatively, substances that can disperse uniformly into the alloy melt as solidified nuclei to promote nucleation can also be added. Modification treatment is less expensive, easier to operate, and more effective compared with the above methods. Adding modifier elements such as calcium (Ca), yttrium (Y), strontium (Sr), cerium (Ce), gadolinium (Gd), neodymium (Nd), barium (Ba), stibium (Sb), tin (Sn) to the magnesium alloy to react with Si element can change the morphologies of both primary and eutectic Mg_2Si phase so as to improve the mechanical properties[21,27-34].

Moussa et al[27] found that adding 0.3wt% Ca to Mg-5Si alloy can effectively reduce the average size of the primary Mg_2Si in the alloy to about 50 μm and transform the phase morphology to polyhedral. This is due to the segregation and "poisoning" of calcium atoms in the alloy[35]. However, excessive addition of calcium results in the formation of massive, needle-like CaMgSi particles, which will destroy the continuity of the alloy matrix. As a result, the modification effect of Mg_2Si is weakened and the alloy properties are degraded. Sb atoms can achieve a similar outcome. Two mechanisms are responsible for it. One is that free Sb atoms can occupy the surface of Mg_2Si crystal and their "poisoning" effect can effectively decrease the size of the primary Mg_2Si. The other involves heterogeneous nucleation of Mg_3Sb_2. This phase is stable and can act as a nucleus for Mg_2Si particle growth. Xiao et al[33] demonstrated this by adding 2.0wt% Sb to the magnesium alloy. It turned out that the average size of the primary phase of Mg_2Si was reduced from 71 μm to 18 μm and the phase morphology transformed from coarse dendrites to massive octahedral. In addition, the intrinsic hardness of Mg_2Si modified by Sb was increased by 36.6% (from 4.21 GPa to 5.75 GPa), and the compressive strength increased from 386 MPa to 415 MPa with an increase in the compressive strain from 14.1% to 16.5%.

Eutectic Mg_2Si can also be modified and Zhang et al[36] found that the coarse Chinese-script-shaped eutectic Mg_2Si in the microstructure can be turned to fine particles by adding Al-P intermediate alloy to AZ91-0.7%Si alloy. Modification effect on eutectic Mg_2Si is realized via various mechanisms. Han et al[37] suggested that adsorption and doping of Nd atoms in the (100) surface in the magnesium alloys permit the modification of the eutectic Mg_2Si phase. In contrast, Ghandvar et al[32] found a different mechanism, i.e. the Al_4Ba compound obtained by adding Ba element to the Al-Mg-Si melt can act as a heterogeneous nucleation core for the primary Mg_2Si phase and the growth of Mg_2Si in the {100} surfaces is inhibited.

However, the majority of existing studies on the modification treatment of Mg_2Si in Al-free magnesium alloys tend to emphasize either the primary phase or the eutectic phase. Although Chen et al[38] did suggest that addition of 1wt% Ba can effectively refine the primary Mg_2Si phase in the microstructure and reduce the amount of eutectic Mg_2Si phase particles, relevant studies are scarce and superficial, lacking excellent modification effect on both phases. Based on these, our study proposed a new composite modification of Ba-Nd, and investigated the modification effect on the microstructure and mechanical properties of high-silicon, Al-free magnesium alloys. The results indicated that Ba-Nd is capable of refining both primary and eutectic phases of Mg_2Si and hence yields excellent mechanical properties.

1 Experiment

1.1 Materials and processing

Commercially pure magnesium (purity≥99.6%) and zinc (purity≥99.5%), Mg-35.2Si master alloy, Mg-10Ba master alloy and Mg-30Nd master alloy were used as raw materials

to prepare the investigated samples of magnesium alloys. All ingredient metals and alloys were calculated and cut according to the chemical composition shown in Table 1. All the materials were preheated to 200 °C and dried. The melting process of the alloy was carried out in a gas-controlled well resistance furnace (SG-7.5-12, 7.5 kW). When the internal temperature reached 500 °C, dried pure magnesium was added into a mild steel crucible (diameter=80 mm, height=250 mm), placed inside the furnace and melted under the protection of mixed SF_6 and CO_2 (0.5 : 100) gases. The furnace was heated continuously to 750 °C and kept until the pure magnesium was completely melted. Then, when the furnace temperature was increased to 790 °C, the Mg-Si master alloy was added three times and the interval time was about 1 h. After the Mg-Si alloy was added every time, the melt was stirred with a stirring bar for 3~5 min for the composition uniformity of the melt and melting efficiency. Pure zinc, Mg-Ba master alloy and Mg-Nd master alloy were added into the melt in turn after complete melting and surface slag removing, stirred for 5 min and then rested for 5 min. Consequently, the prepared melt was cast into graphite mold (diameter=50 mm, height=130 mm) protected by the mixed gas of SF_6 and CO_2.

1.2 Materials characterization

The metallographic specimens were cut from the prepared magnesium alloy samples at the height of 1/3 from the sample bottom and the radius of 1/2 from its axial centre, as seen in Fig.1. The solidification microstructure was observed by optical microscope (OM, Olympus GX71) and the metallographic photos were taken after the specimens were ground and polished. The morphology and microscopic composition of the precipitated phase in the microstructure of the alloy were investigated by scanning electric microscopy (SEM, JSM-6700) equipped with energy dispersive spec-troscopy (EDS). The phase composition of the alloys was measured by X-ray diffraction analysis (XRD, Smartlab) with a diffraction angle from 20° to 90° and a scanning speed of 1°/min to identify the phases in the alloy. The modification mechanism of the alloy melt and its solidification were revealed in combination with optical metallographic microstructure.

1.3 Hardness measuring

The hardness of the alloy specimens was tested using a

Table 1   Chemical composition of Mg-3Si-4Zn-xBa-yNd alloys (wt%)

Alloy No.	Zn	Si	Ba	Nd	Mg
1	4	3	0	0	Bal.
2	4	3	0.8	0	Bal.
3	4	3	1.0	0	Bal.
4	4	3	1.2	0	Bal.
5	4	3	1.5	0	Bal.
6	4	3	1.2	0.8	Bal.
7	4	3	1.2	1.0	Bal.
8	4	3	1.2	1.5	Bal.
9	4	3	1.2	2.0	Bal.
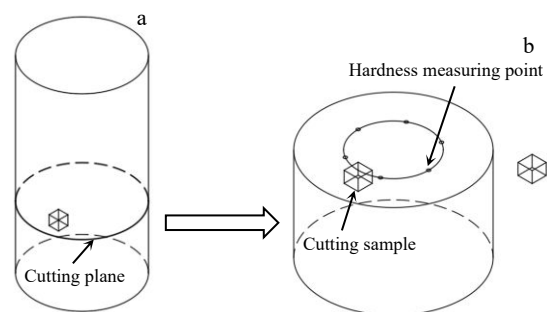
Fig.1   Schematic diagram of cutting metallographic sample: (a) cast sample and (b) cutting sample for metallography and hardness measuring

microhardness tester (DPHV-1000 type) under the testing pressure of 0.98 N and the loading time of 15 s. Six measuring positions were located at the radius of 1/2 from the axial centre of the above cylindrical specimens, which were evenly distributed on the circumstance, as seen from Fig.1b. The data obtained were averaged as the hardness of this specimen except the minimum and maximum.

2 Results

2.1 Modification of single modifier Ba

Based on our results, the size of both primary and eutectic Mg_2Si decreases as the Ba modifier content increases. As shown in Fig. 2 and Fig. 3, the exact size of primary Mg_2Si decreases from approximately 600 μm^2 (40 $\mu m \times 15$ μm) to 178 μm^2 (13.3 $\mu m \times 13.3$ μm), while that of the eutectic Mg_2Si is reduced from 444 μm^2 to 67 μm^2. However, this effect is lost and reversed when the Ba content exceeds 1.2wt%. In addition, the Ba modifier also refines the morphology of both Mg_2Si phases. The shape of the primary Mg_2Si phase is transformed from a dendritic shape (Fig. 2a) to an approximately square shape (Fig.2d). In contrast, the eutectic phase is changed from a complex and coarse Chinese-script shape to a simpler shape (at the upper right corner of Fig.2a and 2d). The best modification effects on both phases occur when the content of Ba reaches 1.2wt%. In the following test of the hardness of the refined alloys, alloys with 1.2wt% Ba shows the greatest hardness (739.41 MPa) in Fig. 4, exhibiting an increase of 28.4% compared with alloy without the Ba modifier (575.75 MPa).

2.2 Composite modification of Ba-Nd

Given that the optimal Ba content is 1.2wt% when the Ba is used as the only modifier, the composite modification of Ba-Nd is assessed by adding Nd (0.8wt%, 1.0wt%, 1.5wt%, 2.0wt%) to Mg-3Si-4Zn-1.2Ba alloy. Again, metallographic micro-graphs of Mg-3Si-4Zn-1.2Ba-xNd alloys are obtained to assess the size and morphology of the Mg_2Si particle (Fig.5).

The size of both Mg_2Si phases further decreases upon the addition of Nd and the optimal effect appears when the Nd content reaches 2.0wt%. Under this experiment condition, the
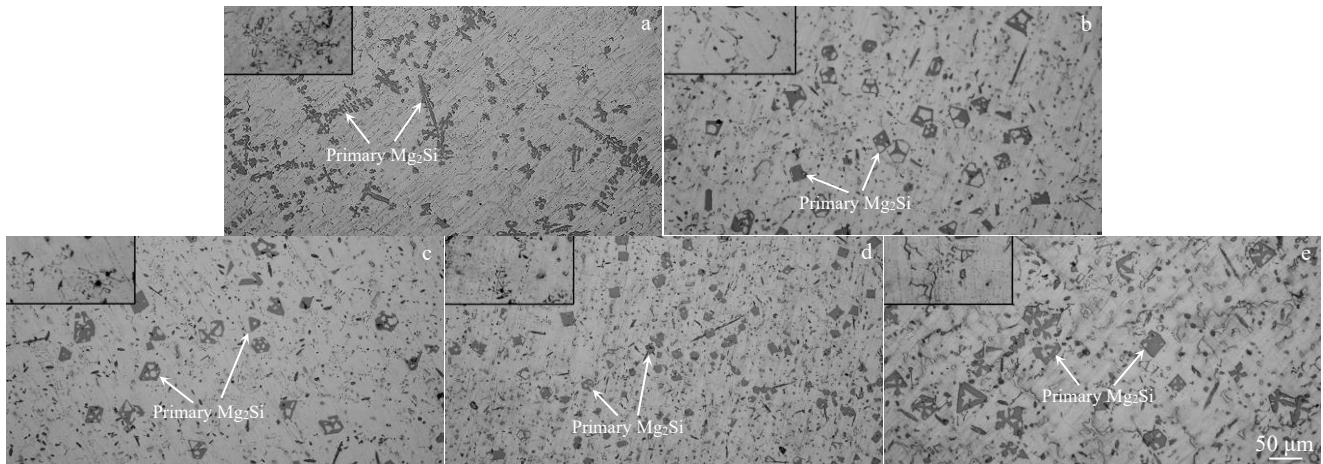
Fig.2   Metallographic microstructures of Mg-3Si-4Zn alloy with different Ba contents: (a) 0wt%, (b) 0.8wt%, (c) 1.0wt%, (d) 1.2wt%, and (e) 1.5wt% (white arrow indicates primary Mg_2Si with block shape; with increasing the Ba content, the primary phase shape changes from dendritic and hollow polygonal block to fine block and then restores hollow polygonal block)
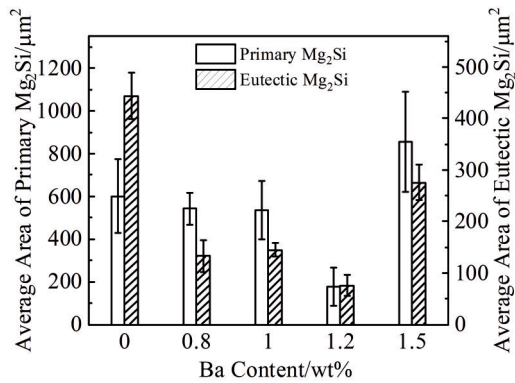
Fig.3   Average area of primary Mg_2Si grains and eutectic Mg_2Si with different Ba contents
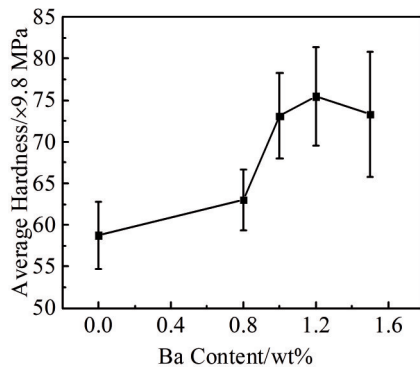
Fig.4   Average hardness values of Mg-3Si-4Zn alloy with different Ba contents

primary Mg_2Si particles are almost invisible in the microstructure (Fig. 5d). In this case, primary Mg_2Si becomes tiny blocks with an average area of about 25 μm^2 (5 $\mu m \times 5$ μm as shown in Fig. 6). Similarly, the size of eutectic Mg_2Si also decreases (Fig. 7) from 356 μm^2 to about 89 μm^2. Although this is slightly larger than that in alloys with Ba modifier alone

(1.2wt%), the size is still significantly reduced. As described above, the composite modification effects of Ba-Nd are best at the Nd content of 2.0wt% and the Ba content of 1.2wt%.

The hardness of Mg-3Si-4Zn-1.2Ba-xNd (x=0.8, 1.0, 1.5, 2.0) is also assessed and the hardness decreases when the Nd content is below 1.5wt% and increases afterwards, as shown in Fig.8.

3   Discussion

3.1   Modification mechanism of Ba

From the above experimental results, we can see that the modification of only adding Ba to the high Si magnesium alloy is different from the composite modification of Ba-Nd. To reveal the modification mechanism, XRD analyses were performed and the results are shown in Fig.9.

From Fig. 9, when Ba is the only modifier, Ba-Si intermetallic phases arise in addition to Mg_2Si phases. Then Fig. 10a indicates that the phases of $BaMg_2Si_2$ (marked as B) grow coherently with Mg_2Si phase, because the needle-shaped $BaMg_2Si_2$ phase grows together with the block of Mg_2Si phase. With these facts identified, it can be concluded that Ba refines the size of Mg_2Si phases, because the $BaMg_2Si_2$ particles can act as a heterogeneous nucleation core for the primary Mg_2Si.

The $BaMg_2Si_2$ particles make the growth of Mg_2Si phases easier; hence more Si atoms are consumed at the early stage of solidification under non-equilibrium solidification conditions. As a result, the Si content in the remaining liquid phase is much lower than that in the Mg-Si eutectic phase and the amount of the eutectic Mg_2Si generated is reduced. However, if the Ba content increases beyond the optimum, the agglomerative growth of $BaMg_2Si_2$ weakens the modification effect. The underlying mechanism is that the $BaMg_2Si_2$ grows into a needle-shaped phase as the Ba content increases. These $BaMg_2Si_2$ phases can no longer be heterogeneous nucleation cores and the modification effects are weakened[38].
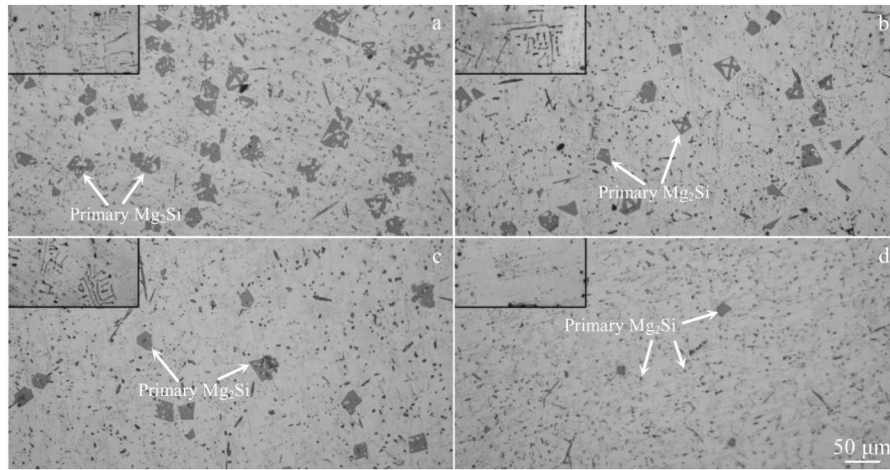
Fig.5　Microstructures of Mg-3Si-4Zn-1.2Ba-*x*Nd with different Nd contents: (a) 0wt%, (b) 1.0wt%, (c) 1.5wt%, and (d) 2.0wt%

Element	wt%	at%
Mg	80.01	83.09
Si	18.07	16.24
Zn	1.56	0.60
Ba	0.36	0.07
Nd	0.00	0.00
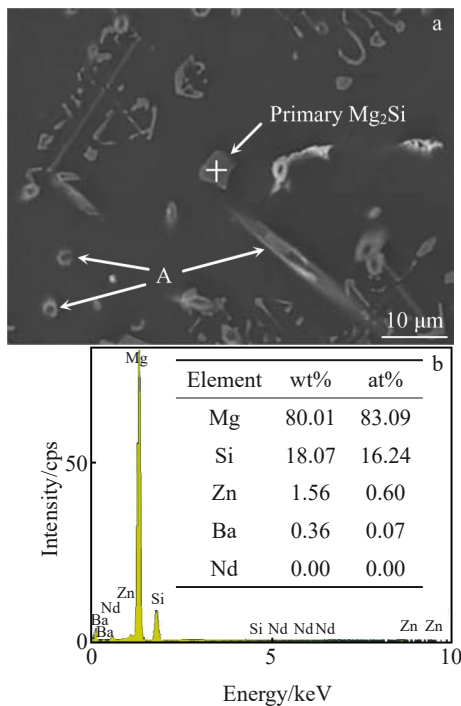
Fig.6　SEM image (a) and EDS results (b) of Mg-3Si-4Zn-1.2Ba-2.0Nd (A presents fine needle-like and hollow ring-like phases discussed at Section 3.2)

Fig.7　Variation of average area of eutectic Mg_2Si with different Nd contents
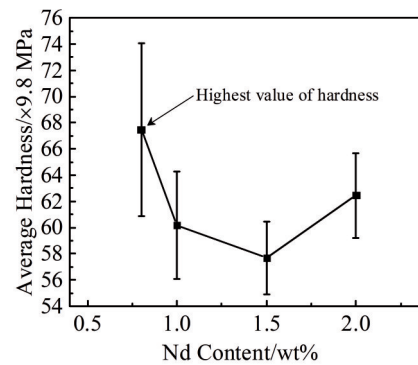
Fig.8　Average hardness values of Mg-3Si-4Zn-1.2Ba alloy with different Nd contents

3.2　Modification mechanism of Ba and Nd

After Nd is added to the Mg-3Si-4Zn-1.2Ba magnesium alloy, the XRD results indicate that the $BaMg_2Si_2$ phases disappear and Ba_2Si, $BaSi_2$, NdSi and $NdSi_2$ phases emerge seen from Fig. 9. As shown in SEM image, many fine needle-like and hollow ring-like phases are found (indicated by A in Fig. 6). Results of line scanning for the phases in Fig. 11 suggest that their main components are Si, Ba and Nd, but no Mg. Therefore, they may be different sections for the same compound. If this XRD result and the Ba-Si, Nd-Si, Ba-Nd phase diagrams[39] (Fig. 12) are considered together, it can be demonstrated that the compounds are Ba_2Si, $BaSi_2$, NdSi and

$NdSi_2$ by comparing the element distribution of Mg, Si, Ba and Nd. Because of the enrichment of Si (Fig. 11d), Ba (Fig. 11e) and Nb (Fig. 11f) of needle-like or ring-like phases and the lack of Mg element (Fig. 11c), compounds of Ba-Si and Nd-Si always ap-pear together.

According to the Miedema model[40], the mixing enthalpy of the binary alloy can be expressed as：

$$\Delta H_{mix} = x_A f_B^A \Delta H_{sol}^{A\,in\,B} \tag{1}$$
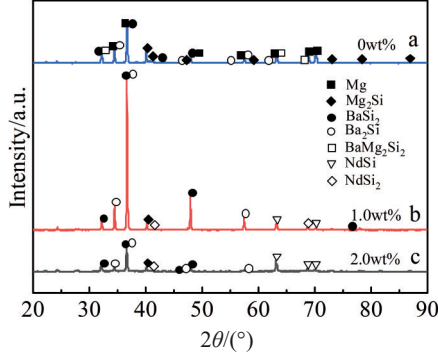
Fig.9   XRD results of Mg-3Si-4Zn-1.2Ba alloy with different Nd contents
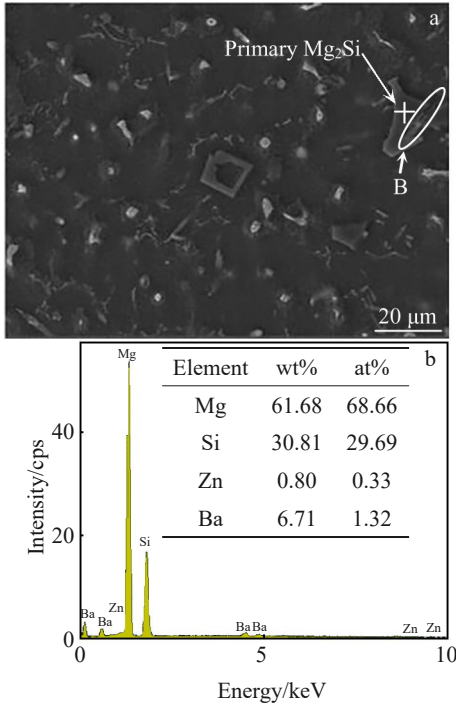
Fig.10   SEM image (a) and EDS results of the point B marked in Fig.10a (b) of Mg-3Si-4Zn-1.2Ba alloy

where $\Delta H_{sol}^{A\,in\,B}$ is the heat of dissolution of element A into element B, which can be calculated by Eq.(2); f_B^A is the ratio of A atoms surrounded by B atoms, which can be calculated by Eq.(3).

$$\Delta H_{sol}^{A\,in\,B} = 2pV_a^{2/3}[1 + \mu_A x_B(\Phi_A^* - \Phi_B^*)]$$
$$\times \frac{\dfrac{q}{p}(\Delta n_{ws}^{1/3})^2 - (\Delta\Phi^*)^2 - \dfrac{R}{p}}{(n_{ws}^{1/3})_A^{-1} + (n_{ws}^{1/3})_B^{-1}} \quad (2)$$

$$f_B^A = \begin{cases} x_B^s \\ x_B^s[1 + 8(x_A^s x_B^s)^2] \end{cases} \quad (3)$$

in which Φ^* is the electronegativity parameter of element; $n_{ws}^{1/3}$ is the average electron densities of element at the Wigner-seitz cell boundary, whose subscript A and B represent element A and B, respectively; μ, q, R and p are empirical parameters, q/p =9.4, and the parameter μ takes different values depending on

the atomic valence of the element[40-42]; x_A^s and x_B^s are the surface concentrations of atom A and B, respectively, calculated as follows:

$$\begin{cases} x_B^s = \dfrac{x_A V_A^{2/3}}{x_A V_A^{2/3} + x_B V_B^{2/3}} \\ x_B^s = \dfrac{x_B V_B^{2/3}}{x_A V_A^{2/3} + x_B V_B^{2/3}} \end{cases} \quad (4)$$

In Eq. (4), V_A and V_B are the atomic molar volumes of element A and B in their alloy, respectively, calculated by Eq.(5).

$$\begin{cases} V_A^{2/3} = V_a^{2/3}[1 + \mu_A x_B(\Phi_A^* - \Phi_B^*)] \\ V_B^{2/3} = V_b^{2/3}[1 + \mu_B x_A(\Phi_B^* - \Phi_A^*)] \end{cases} \quad (5)$$

where V_a and V_b denote the atomic molar volumes of the pure element A and B, respectively.

So, the mixing enthalpy of the disordered binary alloys and ordered alloys can be calculated by Eq. (6) and Eq. (7), respectively, which are obtained by substituting Eq. (2)~(5) into Eq.(1).

$$\Delta H_{mix} = \Lambda_{AB} \frac{x_A V_A^{2/3} x_B V_B^{2/3}}{x_A V_A^{2/3} + x_B V_B^{2/3}} \quad (6)$$

$$\Delta H_{mix}^{order} = \Delta H_{mix}$$
$$\times\left[1 + 8\left(\frac{\Delta H_{mix}}{\Lambda_{AB}\{x_A V_A^{2/3} + x_B V_B^{2/3}\}}\right)^2\right] \quad (7)$$

$$\Lambda_{AB} = 2p\frac{\dfrac{q}{p}(\Delta n_{ws}^{1/3})^2 - (\Delta\phi^*)^2 - \dfrac{R}{p}}{(n_{ws}^{1/3})_A^{-1} + (n_{ws}^{1/3})_B^{-1}} \quad (8)$$

The relationship between the excess Gibbs free energy ΔG_{AB}^E, the excess entropy ΔS_{AB}^E and the heat generation ΔH_{mix} of the binary alloy is as follows:

$$\Delta G_{AB}^E = \Delta H_{mix} - T\Delta S_{AB}^E \quad (9)$$

where T is the absolute temperature of the system (K). Eq.(10) can be got assuming $\Delta S_{AB}^E \approx 0$ since $|\Delta S_{AB}^E| \ll |\Delta H_{mix}|$.

$$\Delta G_{AB}^E = \Delta H_{mix} \quad (10)$$

So, the partial molar excess Gibbs energy ΔG_A^E and ΔG_B^E can be calculated using Eq.(11) and Eq.(12), respectively.

$$\Delta G_A^E = RT\ln\gamma_A = \Delta G_{AB}^E + x_B\frac{\partial\Delta G_{AB}^E}{\partial x_A} \quad (11)$$

$$\Delta G_B^E = RT\ln\gamma_B = \Delta G_{AB}^E - (1 - x_B)\frac{\partial\Delta G_{AB}^E}{\partial x_A} \quad (12)$$

The element activity in the alloy melt is then

$$\alpha_i = \gamma_i x_i \quad (13)$$

where γ is the activity coefficient of the element, and α the element activity, whose subscript i is A or B.

When A_mB_n phase begins to precipitate from the A-B binary alloy melt at T_i, near the liquidus at the alloy composition c_i, $m[A] + n[B] = A_mB_n$ (s) reaction occurs, and its change in the Gibbs free energy ($\Delta G_{T_i}^\theta$) can be calculated by the following relationship[43].

$$\Delta G_{T_i}^\theta = RT_i\ln(\alpha_A^m\alpha_B^n) \quad (14)$$

The relationship between $\Delta G_{T_i}^\theta$ and T_i is shown in Fig.13, calculated with scatter of Eq.(14), and it can be described by Eq.(15) fitted using Origin software.
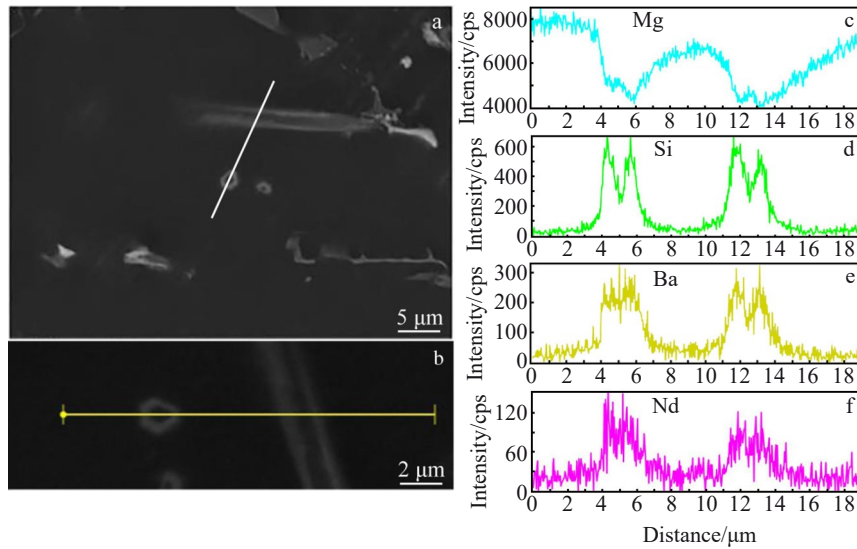
Fig.11   SEM images (a, b) and EDS line scan results along line marked in Fig.11b (c~f) of Mg-3Si-4Zn-1.2Ba-2.0Nd
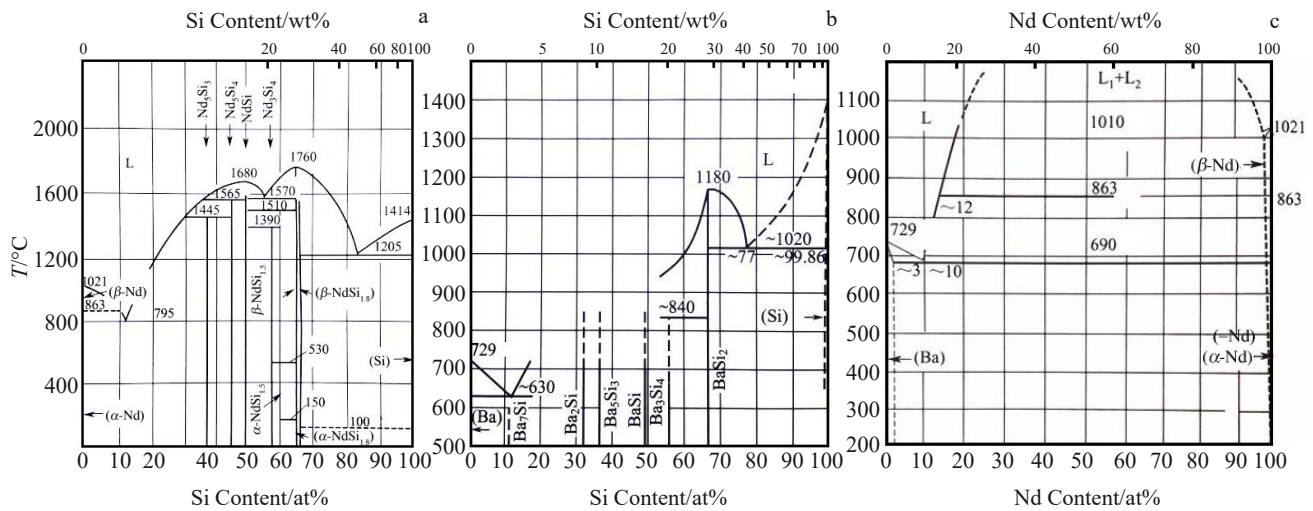
Fig.12   Phase diagram of binary alloy of Nd-Si (a), Ba-Si (b) and Ba-Nd (c)[39]
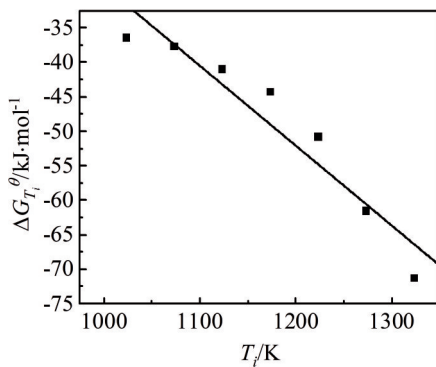
Fig.13   Relationships of $\Delta G_{T_i}^{\theta}$ and T_i for precipitation reaction of Mg$_2$Si in Mg-Si binary alloy

$$\Delta G_T^{\theta} = u + wT \tag{15}$$

where u and w are the fitting constants.

The Gibbs free energy of the Mg$_2$Si phase precipitation reaction is calculated and shown in Fig.13 by selecting seven temperatures T_i in the range of 1023 K to 1323 K from the Mg-Si binary phase diagram, corresponding to the alloy composition c_i. Fitting these scattered points in Fig. 13, Eq.(16) is obtained for the Mg$_2$Si precipitation reaction.

$$(\Delta G^{\theta})_{\text{Mg}_2\text{Si}} = 86976.48132 - 115.889T \tag{16}$$

Similarly, Eq.(17) in the temperature range from 1873 K to 1973 K and Eq.(18) in the temperature range from 1273 K to 1873 K are obtained for the Gibbs free energy of the precipitation reaction of the NdSi$_2$ phase and NdSi phase, respectively. Eq.(19) in the temperature range of 1123~1223 K and Eq. (20) in the temperature range of 913~993 K are obtained for the Gibbs free energy of the precipitation reaction of the BaSi$_2$ phase and Ba$_2$Si phase, respectively.

$$(\Delta G^{\theta})_{\text{NdSi}_2} = -58879.86713 - 27.6681T \tag{17}$$

$$(\Delta G^{\theta})_{\text{NdSi}} = 8900.34385 - 43.25617T \tag{18}$$

$$(\Delta G^{\theta})_{BaSi_2} = 262828.20198 - 349.1423T \tag{19}$$

$$(\Delta G^{\theta})_{Ba_2Si} = 116814.13053 - 189.874127T \tag{20}$$

In the system of the molten Mg-3Si-4Zn alloy with Nd content of 2.0wt% or/and Ba content of 1.2wt% , ΔG^{θ} of forming Ba_2Si, $BaSi_2$, $NdSi$, and $NdSi_2$ compounds are calculated and their relative stability is compared with each other. However, the alloy melting point temperature T_m can be calculated by the following formula[44] because the alloy melt is dilute solution, presuming that the alloy solidifies and crystallizes at the temperature of T_m.

$$T_m = \sum_{i=1}^{n} c_i (T_m)_i \tag{21}$$

where $(T_m)_i$ is the melting point temperature of the alloy component i.

According to Eq. (16)~(20), the Gibbs free energy of forming Mg_2Si, Ba_2Si, $BaSi_2$, $NdSi$, and $NdSi_2$ in the alloy melt are obtained at T_m=941 K which is −22.08, −61.86, −65.71, −31.80 and −84.92 kJ mol^{-1}, respectively. According to thermody-namic knowledge, the larger the absolute value of the Gibbs free energy, the easier the reaction to proceed and the more stable the resulting compound. Therefore, $NdSi_2$ is the most stable compound, followed by $BaSi_2$, Ba_2Si, and $NdSi$, all of which are more stable than Mg_2Si. Therefore, when Ba and Nd are present in the magnesium alloy melt as modifiers, Si atoms originally bound to the Mg in the melt preferentially bond with Nd and Ba during solidification.

When the Nd content is low, the microstructural morphology of Mg_2Si exhibits minor difference from that of alloy with the single Ba modifier (as shown in Fig. 5a and Fig. 2d), because Nd has a high solubility (3.6%) in the magnesium matrix[45]. However, if the Nd content (Fig.5b~5d) increases in the magnesium matrix, Nd atoms will precipitate and interact with other atoms. As a result, primary Mg_2Si in the alloy gradually decreases in size and ultimately "disappears" at the Nd content of 2.0wt%.

According to the above calculated results of free energy and stability order of those compounds, it can be deduced that when Nd is present in the melt, Si atoms will firstly bond to Nd anywhere in the melt and give arise to the $NdSi_2$ phases during the solidification of the alloy melt. As the process proceeds, free Nd atoms decrease rapidly and dramatically. The chemical potential of Nd in the melt decreases sharply and the forming Gibbs free energy change ΔG^{θ} of the reaction between Nd and Si increases obviously. When it is higher than that of the reaction between Ba and Si, Ba atoms bond to Si atoms instead of the reaction of Nd and Si. As the reaction proceeds, the Gibbs free energy ΔG^{θ} for the reaction of Ba and Si increases, and Nd and Si recombine to form NdSi instead of Ba and Si. Similarly, the Gibbs free energy ΔG^{θ} for the reaction of Nd and Si continues to increase, and Mg atoms begin to combine with Si atoms instead of Nd and Si. So, the formed intermetallic compounds of Nd-Si will be dispersed uniformly with the short needle shape because of the strong combining ability (the highest stability of the intermetallic compound) between Nd and Si atoms and the short reaction

time. As the temperature decreases, the peritectic reactions, such as L+NdSi→Nd_5Si_4, L+Nd_5Si_4→Nd_5Si_3, will take place according to the phase diagram of Nd-Si (as seen in Fig.12a). But these reactions do not occur because Nd_5Si_4, Nd_5Si_3, etc are not found in Fig.9b and Fig.9c. So, the Nd-Si intermetallic compounds are stable in the melt when the reaction of Ba and Si begins. According to the phase diagram of Ba-Nd (as seen in Fig.12c), Ba and Nd have a greater mutual solubility at high temperature, but no any intermetallic compounds form. It is easier to form Ba-Si compounds attached to the Nd-Si intermetallic compound as seen from Fig. 11d~11f. These reactions consume a large number of Si atoms. It is the "robbery" of Si atoms by Nd and Ba atoms, which causes insufficient Si atoms during the growth of primary Mg_2Si and restricts the development of primary Mg_2Si in a preferential direction of {100}. These further contribute to the uniform distribution of the Mg_2Si with a tiny squared shape in the alloy matrix.

The modification mechanism of Ba-Nd composite on eutectic Mg_2Si has been revealed by the previous research. Han et al[37] suggested that the main mechanism of Nd modification on the eutectic Mg_2Si phase in magnesium alloys may be the surface adsorption, by which Nd atoms are preferentially adsorbed to the vacant sites on the {100} surface of eutectic Mg_2Si, but not the H_2 sites on the {111} surface. This is because the adsorption energy of rare-earth Nd atoms on the {100} surface of Mg_2Si is much smaller than that on the {111} surface. The crystal growth of the {100} preferential growth surface of Mg_2Si is inhibited by the covering of the easily absorbed rare-earth Nd atoms on the {100} surface. Moreover, Nd atoms have a strong doping effect on the {100} surface of Mg_2Si, which is justified by calculating the doping and adsorption properties of Nd on the Mg_2Si surfaces of {100} and {111} using the first-principles approach[37]. The two factors of doping and adsorption of Nd on the {100} surface of eutectic Mg_2Si reduce the average area of Mg_2Si. The composite modifier Ba-Nd can also reduce the size and quantity of eutectic Mg_2Si, as discussed in the Section 3.1.

To sum up, the size and morphology of the primary and eutectic Mg_2Si can be changed effectively by the composite modification of Ba-Nd.

3.3 Role of Mg_2Si phase on the alloy hardness

The highest hardness of the alloy containing Nd does not appear at the Nd content of 2.0wt% (612.11 MPa), but it appears when the Nd content reaches 0.8wt% at the Ba content of 1.2wt% . The alloy hardness decreases with increasing the Nd content, reaching the lowest value (575.75 MPa) at the Nd content of 1.5wt% in the experiments. Afterwards, hardness begins to increase. Microstructural analyses were performed and the changes of the size and the number of the primary Mg_2Si and eutectic Mg_2Si are schematically shown in Fig.14. The size and the number of the primary Mg_2Si phases decrease, while the size of the eutectic Mg_2Si decreases and the number increases as the Nd content increases. When the Nd content is low, primary Mg_2Si plays
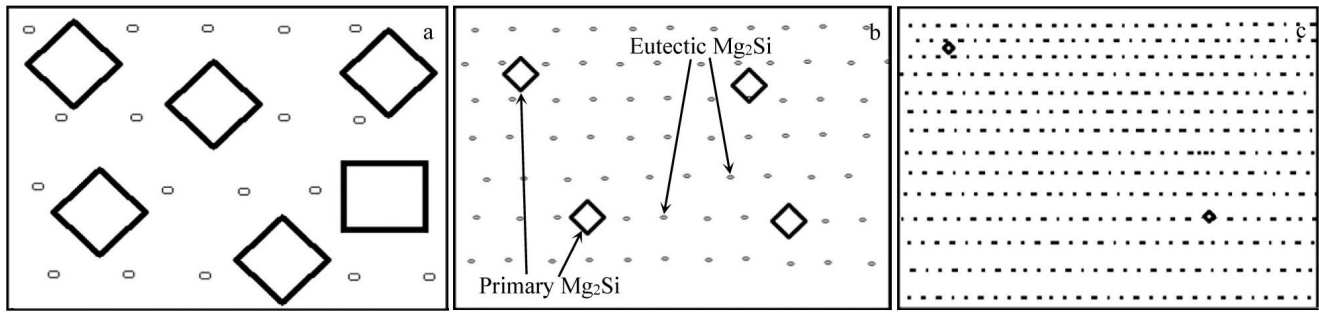
Fig.14   Schematic diagram of changes of size and distribution of the primary and eutectic Mg_2Si in the alloy microstructure with Nd content at the Ba content of 1.2wt% according to Fig. 5: (a) coarsening of primary Mg_2Si and sparse eutectic Mg_2Si, (b) decrease of primary Mg_2Si size and increase of eutectic Mg_2Si, and (c) disappearing of primary Mg_2Si and increased distributed eutectic Mg_2Si

an important role in measuring the hardness because the indenter of hardness tester has a greater possibility to be pressed due to its large size. However, when the Nd content increases, the contribution of the primary phase to the alloy hardness decreases and that of the eutectic phase increases. The alloy hardness decreases until the contribution of the eutectic phase is dominant.

3.4 Properties and application of high Si magnesium alloy after Ba-Nd composite modification

As mentioned before, it is very difficult to obtain the alloy microstructure with fine particles and uniform dispersion of Mg_2Si, especially when the Si content is high. Many studies showed that the size of primary Mg_2Si decreases and its morphology changes from coarsen dendritic shape to small block shape, but the size is almost always greater than 15 μm and the shape is sharp. But in this experiment, as shown in Fig. 5d and Fig. 6a, primary Mg_2Si becomes tiny blocks with an average area of about 25 $μm^2$ (5 μm×5 μm) and the size of eutectic Mg_2Si decreases (Fig. 7) to about 89 $μm^2$ by adding 1.2wt% Ba and 2.0wt% Nd.

According to the relationship between microstructure and properties, the microstructure of the alloy will determine its outstanding room-temperature properties in spite that its hardness is not the highest. This is consistent with the good high-temperature properties of the alloy (the room-temperature and high-temperature properties will be reported in the future). Tiny particles of primary Mg_2Si will enhance the room-temperature tensile strength of the alloy compared with the coarsen Mg_2Si dendrite, since the pinning dislocation prevents it from moving. At the same time, ductility of the alloy also increases due to the fine crystals of Mg_2Si. At elevated temperatures, these fine particles of Mg_2Si can also prevent the alloy matrix crystal boundaries from travelling and this improves creep resistance and high-temperature strength. Overall, the high Si magnesium alloys after composite modification may develop good comprehensive mechanical properties at both room temperature and high temperature.

The high Si magnesium alloys are more prone to

deformation after Ba-Nd composite modification because of the improved ductility. Deformation of the alloys will crush the matrix crystal grains and the tiny particles of Mg_2Si into smaller pieces. As a result, it is possible to achieve a magnesium matrix composites with uniformly dispersed tiny Mg_2Si particles, which are reinforced and can be deformed easily.

4 Conclusions

1) The best modification effect can be achieved by adding 1.2wt% Ba to the Mg-3Si-4Zn alloy melt, with the primary Mg_2Si changing from dendrites with an average area of about 600 $μm^2$ (40 μm×15 μm) to nearly square with an average area of about 178 $μm^2$ (13.3 μm×13.3 μm). The eutectic Mg_2Si with Chinese-script shape is changed from complex and coarse with an average area of about 444 $μm^2$ to a simple dotted-line with area of about 67 $μm^2$. The hardness value of the alloy is increased by 28.4% from 575.75 MPa to 739.41 MPa. However, when the Ba content is greater than 1.2wt%, the mechanical properties of the alloy are limited by excessive modification due to the generation of excessive needle-like $BaMg_2Si_2$.

2) At the optimal Ba content of 1.2wt%, the size of primary Mg_2Si in the microstructure gradually decreases with an increase in the Nd content, and the eutectic Mg_2Si with the Chinese-script shape is changed from complex with the average area of about 356 $μm^2$ to simple with a mean area of about 89 $μm^2$. The best modification effects are achieved, in which the primary Mg_2Si is changed into the tiny square block shape with the length of about 5 μm when the compound modifier has a Ba content of 1.2wt% and an Nd content of 2.0wt% . Under the composite modification, the hardness value of the alloy increases from 575.75 MPa to 612.11 MPa, increased by 6.31%.

3) When Ba-Nd is added as a composite modification agent, the growth of primary Mg_2Si phase is inhibited and its size becomes smaller because Nd and Ba atoms can bond to Si atoms prior to Mg atoms according to the calculated results of the stability of $NdSi_2$, $BaSi_2$, Ba_2Si, $NdSi$ and Mg_2Si phases

from the Miedema model.

References

1 Pan F S, Yang M B, Chen X H. *Journal of Materials Science & Technology*[J], 2016, 32(12): 1211

2 Spigarelli S, Cabibbo M, Evangelista E *et al*. *Materials Science and Engineering*[J], 2000, 289A(1-2): 172

3 Roodposhti P S, Sarkar A, Murty K L. *Materials Science and Engineering*[J], 2015, 626A: 195

4 Joost W J, Krajewski P E. *Scripta Materialia*[J], 2017, 128: 107

5 Parrish A, Rais-Rohani M, Najafi A. *International Journal of Crashworthiness*[J], 2012, 17(3): 259

6 Luo A A. *International Materials Reviews*[J], 2004, 49(1): 13

7 Pantelakis S G, Alexopoulos N D, Chamos A N. *Journal of Engineering Materials and Technology*[J], 2007, 129: 422

8 Du J, Iwai K, Li W F *et al*. *Transactions of Nonferrous Metals Society of China*[J], 2009, 19(5): 1051

9 Bazhenov V E, Koltygin A V, Sung M C *et al*. *Journal of Magnesium and Alloys*[J], 2020, 8(1): 184

10 Xu C, Nakata T, Ho-ishi K *et al*. *Scripta Materialia*[J], 2017, 139: 34

11 Luo A A, Pekguleryuz M O. *Journal of Materials Science*[J], 1994, 29(20): 5259

12 Li Dongsheng, Cheng Xiaonong. *Materials Review*[J], 2006, 20(VI): 424 (in Chinese)

13 Han F Y, Wang P, Tian L H *et al*. *Rare Metal Materials and Engineering*[J], 2013, 42(7): 1497

14 Li J L, Chen R S, Ma Y Q *et al*. *Journal of Magnesium and Alloys*[J], 2013, 1(4): 346

15 Milkereit B, Burgschat L, Kemsies R H *et al*. *Journal of Magnesium and Alloys*[J], 2019, 7(1): 1

16 Li C, Wu Y Y , Li H *et al*. *Acta Materialia*[J], 2011, 59(3): 1058

17 Meng F B, Huang H J, Yuan X G *et al*. *China Foundry*[J], 2020, 17(1): 15

18 Wang Yanli, Guo Xuefeng, Huang Dan *et al*. *Foundry Technology*[J], 2011, 32(8): 1092 (in Chinese)

19 Liu Jie, Qi Wenjun, Deng Yun *et al*. *Foundry Technology*[J], 2011, 32(9): 1291 (in Chinese)

20 Jiang Q C, Wang H Y, Wang Y *et al*. *Materials Science and Engineering A*[J], 2005, 392(1-2): 130

21 Chen L, Wang H Y, Li Y J *et al*. *CrystEngComm*[J], 2014, 16(3): 448

22 Qin Q D, Zhao Y G, Zhou W *et al*. *Materials Science and Engineering A*[J], 2007, 447(1-2): 186

23 Kou Shoupeng. *Thesis for Master*[D]. Changchun: Changchun University of Technology, 2016 (in Chinese)

24 Wang Yang, Zhang Xiuqing, Chen Ge *et al*. *Hot Working Technology*[J], 2013, 42(8): 163 (in Chinese)

25 Daneshifar M H, Papi A, Alishahi M. *Materials Letters*[J], 2021, 282: 128 832

26 Seth P P, Singh N, Singh M *et al*. *Journal of Alloys and Compounds*[J], 2020, 821: 153 205

27 Moussa M E, Waly M A, El-Sheikh A M. *Journal of Magnesium and Alloys*[J], 2014, 2(3): 230

28 Wang H Y, Zhu J N, Li J H *et al*. *CrystEngComm*[J], 2017, 19(42): 6365

29 Hu B, Zhu W J, Li Z X *et al*. *Journal of Magnesium and Alloys*[J], 2021

30 Ghandvar H, Idris M H, Abu Bakar T A *et al*. *Journal of Materials Research and Technology*[J], 2020, 9(3): 3272

31 Wu X F, Zhang G G, Wu F F. *Rare Metals*[J], 2013, 32: 284

32 Ghandvar H, Jabbar K A, Idris M H *et al*. *Journal of Materials Research and Technology*[J], 2021, 11: 448

33 Xiao P, Gao Y, Mao P *et al*. *Journal of Alloys and Compounds*[J], 2021, 850: 156 877

34 Hu T, Wang F, Zheng R X *et al*. *Journal of Alloys and Compounds*[J], 2019, 796: 1

35 Cong M Q, Li Z Q, Liu J S *et al*. *Journal of Alloys and Compounds*[J], 2012, 539: 168

36 Zhang Jinshan, Gao Yibin, Pei Lixia *et al*. *The Chinese Journal of Nonferrous Metals*[J], 2006, 16(8): 1361 (in Chinese)

37 Han W D, Li Y H, Li X D *et al*. *Applied Surface Science*[J], 2020, 503: 144 331

38 Chen K, Li Z Q, Liu J S *et al*. *Journal of Alloys and Compounds*[J], 2009, 487(1-2): 293

39 Liangkishev H N, Guo Q W. *Handbook of Phase Diagrams of Metal Binary Systems*[M]. Beijing: Chemical Industry Press, 2009

40 Deboer F R, Boom R, Mattens W C M *et al*. *Cohesion in Metals*[M]. Amsterdam: North-Holland, 1988

41 Miedema A R, Chtel P F D, Boer F. *Physica B+C*[J], 1980, 100(1): 1

42 Miedema A R. *Journal of the Less Common Metals*[J], 1973, 32(1): 117

43 Wu Yufeng, Du Wenbo, Nie Zuoren. *Acta Metallurgica Sinica*[J], 2005, 42(5): 487 (in Chinese)

44 Yin Kexin, Wu Baolin, Wang Dapeng *et al*. *Journal of Shenyang Aerospace University*[J], 2015, 32(3): 25 (in Chinese)

45 Hu J L, Tang C P, Zhang X M *et al*. *Transactions of Nonferrous Metals Society of China*[J], 2013, 23(11): 3161

Ba-Nd复合变质对Mg-3Si-4Zn铸造合金组织及性能的影响

童文辉[1]，赵晨爔[1]，童方泽[3]，蔡　倩[2]，黄博男[1]，王　杰[1]，刘昀怿[1]

(1. 沈阳航空航天大学 材料科学与工程学院，辽宁 沈阳 110136)

(2. 沈阳育成鑫科技成果转化技术服务有限公司，辽宁 沈阳 110004)

(3. 剑桥大学 莫里爱德华学院，英国 剑桥 CB3 0DF)

摘　要：研究了Ba-Nd复合变质对Mg-3Si-4Zn铸造合金组织及力学性能的影响，用OM、SEM、EDS、XRD等方法对微观结构进行了表征，通过硬度测试研究了材料的力学性能。结果表明，当单一变质剂Ba在Mg-3Si-4Zn合金中的添加量为1.2%（质量分数）时，变质效果最好。形成的$BaMg_2Si_2$相可以作为初生Mg_2Si的异质形核核心，使初生Mg_2Si细化。Ba-Nd复合变质是通过在Mg-3Si-4Zn-1.2Ba合金中加入变质剂Nd来完成的。通过Miedema模型和对吉布斯自由能的线性拟合，发现由于Nd和/或Ba原子能与Si原子形成更加稳定的化合物$NdSi$、$NdSi_2$、Ba_2Si、$BaSi_2$，防止Si原子在凝固的初始阶段与Mg原子结合，因此初生Mg_2Si的生长速度被抑制，微观结构中初生Mg_2Si相变小。当Nd含量为2.0%时，Ba-Nd复合变质效果最好，即初生Mg_2Si由平均面积约为600 μm^2的树枝状变为平均边长约5 μm的近似方形的组织，共晶Mg_2Si由平均面积约444 μm^2的复杂粗大汉字状变为平均面积约89 μm^2的简单汉字状组织。合金硬度由575.75 MPa提高到612.11 MPa，提高了6.31%。

关键词：Mg-Si-Zn合金；Mg_2Si；Ba-Nd复合变质；组织；硬度；Miedema模型

作者简介：童文辉，男，1971年生，博士，副教授，沈阳航空航天大学材料科学与工程学院，辽宁 沈阳 110136，电话：0086-24-89728968，E-mail：20140013@sau.edu.cn